

Double phase-conjugate mirror: convection and diffraction

A. A. Zozulya, M. Saffman,* and D. Z. Anderson

*Department of Physics and Joint Institute for Laboratory Astrophysics,
University of Colorado, Boulder, Colorado 80309-0440*

Received January 11, 1994; revised manuscript received September 15, 1994

Development of scattered radiation in the geometry of a double phase-conjugate mirror is investigated numerically in the framework of a two-dimensional model that accounts for both diffraction and noncollinearity of the interacting beams. The large-scale structure of the scattered beams is found to be distorted because of the convective flow of energy out of the interaction region. We show that the output characteristics of the double phase-conjugate mirror depend strongly on the level of seed radiation in the direction of the scattered beams. The seed radiation may be due to incoherent scattering of the pumping beams inside the medium or to self-broadening of the pumping beams' spectra because of nonlinear self-interaction.

1. INTRODUCTION

The double phase-conjugate mirror (DPCM) is a self-pumped four-wave mixing geometry in which two mutually incoherent noncollinear pump beams intersect in a photorefractive nonlinear medium (Fig. 1). Two scattered beams are generated that are counterpropagating to the pumps and are their phase-conjugate replicas. A one-dimensional analysis^{1,2} indicates that the DPCM is an oscillator. This means that, once the gain-length product γl exceeds its threshold value γl_{th} , scattered beams start to grow exponentially in time from arbitrarily small values of boundary and/or initial values of seeds. The growth is eventually saturated because of depletion of the pumping beams. The characteristics of the final steady state are determined by the value of γl , and they do not depend on the values of the seeds unless the seeds are very large. This is why the nonlinear characteristics of the DPCM are calculated in the framework of a one-dimensional model^{1,2} with the seeds set to zero. The physics of these results stem from the fact that in a one-dimensional model all interacting beams are assumed to be plane waves of infinite transverse extent (along coordinate y in Fig. 1). The interaction region also has infinite transverse extent, and any physical effects connected with the y coordinate are by definition absent. Under these conditions equations for the scattered beams describe a pair of parametrically coupled waves effectively counterpropagating along the only remaining coordinate x across the nonlinear medium. As is well known (see, e.g., Ref. 3), such a system exhibits an absolute (oscillation) instability.

In reality, all interacting beams have finite diameters, and the interaction region is bounded in all directions. The two-dimensional geometry, combined with noncollinearity of the beams, results in a completely different physics.⁴⁻⁷ The noncollinear scattered beams have both opposite and common components of group velocities. Convective transport of the energy of the scattered beams in the direction of this common compo-

nent (along y in Fig. 1) creates a channel of losses out of the finite-sized interaction region. This loss mechanism is absent in the one-dimensional model because nothing is assumed to change along the transverse coordinate. There is therefore no coordinate-dependent transverse flow responsible for energy loss in the one-dimensional model. In a two-dimensional model the only mechanism that can potentially counterbalance the convective loss of energy is diffraction, returning part of the energy of the beams to the interaction region (down along y in Fig. 1). The relative strength of diffraction is determined by the characteristic diffraction divergence $\delta\theta$ of the pumping beams, whereas the magnitude of convective losses is determined by the magnitude of the angle θ between the pumping beams and their respective copropagating scattered beams (the noncollinearity angle). Experimental realizations of the DPCM correspond to the situation in which $|\theta| > \delta\theta$, such that convection is stronger than diffraction. The opposite situation in which $|\theta| < \delta\theta$ has not been experimentally demonstrated because in this case the spectra of the pumping and the scattered beams are strongly overlapped, which renders the beams not easily separable. When $|\theta| > \delta\theta$ the convective losses quench the absolute (oscillation) instability, and the DPCM is an amplifier. Consequently the steady-state level of scattering is directly dependent on the level of the seeds and goes to zero when the seeds are switched off. In this case the DPCM is similar to stimulated Brillouin scattering, for example, or to incoherent photorefractive scattering (fanning). The analogy, however, ends here. The output level of scattered radiation for both stimulated and Brillouin scattering fanning is proportional to the input level of seeds ϵ times a one-pass amplification coefficient: $\epsilon \exp(2\gamma l)$. In the case of the DPCM the output level has a different dependence on the level of nonlinearity. Its functional form is slightly different for two limiting cases corresponding to the pumping-beam overlap region lying either fully inside the medium or mostly outside it.⁴⁻⁶ For example, analysis of the spatial structure of the scattered beams in the above-mentioned

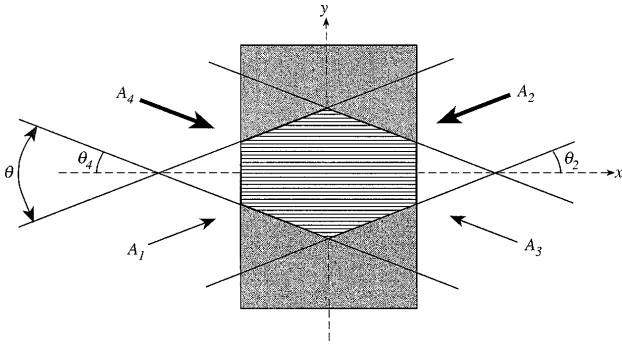


Fig. 1. Geometry of the DPCM.

case of quasi-one-dimensional geometry in which the relative displacement of the beams over the length of the nonlinear medium is small, $\theta l/d \leq 1$ (l is the length of the nonlinear medium and d is the characteristic transverse size of the beams) shows that when the gain-length product γl exceeds its one-dimensional threshold value γl_{th} the scattered beams start to grow in space in the direction of the common component of their group velocities. In other words, in the two-dimensional model of the DPCM, γl_{th} is the threshold of the transverse convective instability. Below, for convenience, we refer to the direction of this common component by the coordinate y , simply because under typical conditions all the angles of incidence of the beams on the nonlinear medium are small. One should remember, however, that the direction of convective growth of the scattered radiation is determined not by the boundaries of the medium but by the group velocities of the beams. This effect is especially clear in the case in which the pumping-beam overlap region (interaction region) lies fully inside the medium because in this case the position of the medium boundaries does not matter at all. For the simplest case of constant-intensity pumping beams the intensities of the scattered beams in the undepleted-pump approximation are proportional to $\epsilon \exp(2py)$, where the growth rate p is a root of the equation⁶

$$(\gamma - p\theta)\tanh(Ql/2) = Q. \quad (1)$$

Here $Q = [(\gamma - p\theta)^2 - 4\gamma^2 q(1 + q)^{-2}]^{1/2}$, where q is the pumping-beam intensity ratio.

Asymptotic solutions of Eq. (1) for equal-intensity pumps $q = 1$ in the limit $|\gamma l - 2| \ll \gamma l$ yield $p = (\gamma l - 2)/\theta l$ and in the limit $\gamma l \gg 1$ yield $p = (2\gamma l - 2\pi^2/\gamma l)/\theta l$. Equation (1) indicates that the output intensity distributions of the scattered beams are shifted with respect to the intensity distributions of the counterpropagating pumps in the direction of the convective flow of energy. When the pumping beams bear images this effect manifests itself in large-scale distortions of the envelopes of the interacting beams, whereas the small-scale structure in the pumping beams is reproduced.

Output powers of the scattered beams in the one-dimensional model are uniquely determined by the value of the nonlinearity γl . In the two-dimensional model according to Eq. (1) they depend on the level of seeds ϵ , the nonlinearity γl , the angle between the beams θ , and their diameters d . Define the characteristic diameter $d_*(\gamma l, \theta, \epsilon) \approx \ln(1/\epsilon)/2p$. If the diameters of the pump

beams d are such that $d < d_*$, the output powers of the scattered beams according to Eq. (1) are proportional to $\epsilon \exp(2pd)$. In the case of wide beams and/or large seeds $d > d_*$ and, consequently, $\epsilon \exp(2pd) \gg 1$, the intensities of the scattered beams first grow with the transverse coordinate moving in the direction of the convective flow of energy, starting from the edge of the interaction region ($y = 0$). The growth then saturates because of pumping-beam depletion at the distance $y \approx d_*$. For $y > d_*$ the local values of intensities will more or less coincide with those given by the one-dimensional model. Note that despite this fact the physics of the appearance of scattered radiation remains quite different in the framework of one- and two-dimensional models. Even the possibility of a limiting transition between the two models is based on keeping the value of d_* (and, consequently, the level of seeds) in the two-dimensional model finite.

Another consequence of Eq. (1) may be seen in the dependence of the nonlinear transmissivities on the value of γl . In the one-dimensional model larger values of γl correspond to larger output. The coupling constant γ in a photorefractive medium is dependent on the angle θ between the pumping beams and has a maximum for some value of $\theta = \theta_D$. It means that in the framework of a one-dimensional model the transmissivities of the DPCM are maximum when the pumping beams are aligned such that the magnitude of the angle θ is equal to θ_D . The two-dimensional model⁴⁻⁶ predicts that this optimum angle is less than θ_D or, in other words, that the maximum transmissivities do not correspond to maximum values of $\gamma(\theta)l$. Indeed, according to Eq. (1) the maximum transmissivities (at least for their low levels near the observable threshold of scattering) correspond not to the maximum of the coupling constant $\gamma(\theta)l$ but to the maximum of the transverse growth rate p that is attained for $\theta < \theta_D$.

The two-dimensional model of Refs. 4-6 neglects diffraction. This paper is devoted to numerical investigation of the physics of development of scattered radiation in the geometry of the DPCM, including the effect of finite transverse size, noncollinearity of the interacting beams, and diffraction. The structure of the paper is as follows: Section 2 deals with the mathematical formulation of the problem, and Section 3 contains a discussion of the numerical results. Section 4 summarizes the results of this study and comments on other recent papers⁸⁻¹² on the same topic.

2. MATHEMATICAL FORMULATION OF THE PROBLEM

The paraxial equations governing propagation of optical beams in the geometry of the DPCM have the form

$$\left(\frac{\partial}{\partial x} - \frac{i}{2k} \frac{\partial^2}{\partial y^2} \right) A_f = 2i\gamma_0 \nu A_f, \quad (2a)$$

$$\left(-\frac{\partial}{\partial x} - \frac{i}{2k} \frac{\partial^2}{\partial y^2} \right) A_b = 2i\gamma_0 \nu A_b, \quad (2b)$$

where k is the wave number of radiation inside the medium; $A_f = A_1 + A_4$ and $A_b = A_2 + A_3$ are forward- and backward-propagating beams, respectively (the

angles of incidence of all beams on the medium are assumed to be small); γ_0 is the nonlinearity constant; and ν is the normalized amplitude of the grating obeying the equation^{13–15}

$$I^{-1} \left(1 + \frac{1}{k\theta_D} \frac{\partial \nu}{\partial y} \right) \frac{\partial}{\partial t} \nu + \nu - \frac{1}{(k\theta_D)^2} \frac{\partial^2 \nu}{\partial y^2} \times \left(1 + \frac{1}{k\theta_D} \frac{\partial \nu}{\partial y} \right)^{-1} = -\frac{1}{k\theta_D} \frac{\partial}{\partial y} \ln I. \quad (3)$$

Here $\theta_D = k_D/k$, where k_D is the Debye wave number, determined by the material parameters of the photorefractive medium,¹³ and $I = |A_f|^2 + |A_b|^2 + I_{er}$ is the sum of intensities of the beams plus a (possible) erasure intensity. The latter term may also be thought of as the equivalent intensity connected with dark conductivity. Equation (3) is based on the assumption that the grating varies most rapidly along the y axis because of the small angles of incidence of all beams on the medium.

When the medium is illuminated by two plane waves A_1 and A_4 ($|A_1| \ll |A_4|$) propagating at an angle θ to each other, the weak wave A_1 grows exponentially in space $\{A_1 \sim \exp[\gamma(\theta)x]\}$ from its boundary value, with the growth rate¹³

$$\gamma(\theta) = \gamma_0 \frac{2(\theta/\theta_D)}{1 + (\theta/\theta_D)^2}. \quad (4)$$

The angle θ_D is thus the angle between plane-wave pump and signal beams corresponding to the maximum coupling between them, and γ_0 is the value of this coupling. The boundary conditions for the system of Eqs. (2) and (3) correspond to specification of input amplitude distributions of the pump beams $A_{4,in}(y)$, $A_{2,in}(y)$ plus random noise at some small level serving as seeds for the appearance of scattered beams. We tried several types of random seeding, including Gaussian, parabolic, and uniform random seeding in Fourier space. All these gave essentially the same results, provided that the noise was sufficiently broadband. The calculations presented below use random uniform seeding in Fourier space covering the whole calculation window. We used both speckled beams and beams with regular structure as input pumping beams. The general form of the input pumping beams corresponded to a form factor $B_{l,in}(y)$ multiplied by a Gaussian envelope plus an exponent giving the mean direction of propagation of the beam:

$$A_{l,in}(y) = B_{l,in}(y) \exp[-i\theta_l ky - 4(y - y_l)^2/d^2]. \quad (5)$$

Here θ_l is the signed angle of incidence of the l th pump beam ($l = 2, 4$), a positive value of θ_l corresponds to a pumping beam with a negative component of group velocity in the y direction, d is the characteristic diameter of the beam, and y_l is the nominal position of its center. The angle between each pump and its copropagating signal θ is given by $\theta = \theta_2 + \theta_4$. For beams with regular structure we used $B_{l,in}(y) \propto \alpha + \beta \cos(\delta y + \psi)$, with different values of parameters α , β , δ , and ψ (periodically modulated Gaussian beams). For speckled beams the form factor $B_{l,in}(y)$ was chosen to be a statistically uniform speckled field with a randomly generated Fourier

spectrum of compact support, corresponding to a given angular divergence $\delta\theta$.

The integral output characteristics of the geometry under consideration are characterized by the transmissivities from right to left (T_{rl}) and from left to right (T_{lr}) according to the relations $T_{lr} = P_{1,out}/P_{4,in}$ and $T_{rl} = P_{3,out}/P_{2,in}$, where $P_{j,in/out}$ are input/output powers of the j th beam, and by the conjugation fidelities H_r and H_l determined by the relations

$$H_l = \frac{\left| \int dy A_{3,out}(y) A_{4,in}(y) \right|^2}{\left[\int dy |A_{3,out}(y)|^2 \right] \left[\int dy |A_{4,in}(y)|^2 \right]}, \quad (6a)$$

$$H_r = \frac{\left| \int dy A_{1,out}(y) A_{2,in}(y) \right|^2}{\left[\int dy |A_{1,out}(y)|^2 \right] \left[\int dy |A_{2,in}(y)|^2 \right]}. \quad (6b)$$

Equations (2) treat pairs of copropagating pumping and scattered beams as single fields without separating them. Below we are interested mainly in conditions for which the pumping-beam overlap region is not completely immersed inside the medium but has a diamond-shaped form (see Fig. 1) and lies partially inside and partially outside the medium. In this case the output scattered beams are spatially overlapped with copropagating pumps at the faces of the nonlinear medium. Retrieval of spatial profiles of the beams was made on the basis of their far-field distributions (Fourier spectra). In the calculations below, the characteristic angular divergences $\delta\theta$ of the input pumping beams are less than the angle θ between them. This result implies that the Fourier spectra of the scattered beams and the copropagating pumps are separated in Fourier space, provided that the scattered beams turn out to be more-or-less faithful phase-conjugate replicas of the pumps. To separate the scattered beams from the copropagating pumps we used a window in Fourier space centered at the spatial frequency corresponding to the nominal direction of propagation of the respective scattered or pumping beam (see Fig. 1), with the width of the window being either equal to or several times the largest characteristic angular divergence of either input pump. All the radiation inside this window is considered to be a scattered (or a pumping) beam. The coordinate distributions of the beams are obtained by calculation of the inverse transform of the spectrum inside the window.

Equations (2) and (3) were solved either by a finite-difference Crank–Nicholson-type scheme¹⁶ with absorption–refraction layers at the boundaries of the computation region in the y direction¹⁷ or by a fast Fourier transform (FFT). Double-precision (64-bit) arithmetic was used for all the numerical calculations. The Crank–Nicholson scheme was used to solve Eq. (3) both in accounting for the nonlinear term $[1 + (k\theta_D)^{-1} \partial \nu / \partial y]$ and in a linearized version in which this term is replaced by unity. Runs both with and without the nonlinear term indicated that it did not result in any significant changes in the behavior of the DPCM. The FFT method was applied only to the linearized form of Eq. (3). The

Crank–Nicholson- and FFT-based numerical results were in good agreement. To keep numerical demands at a reasonably low level the calculations were carried out with scaled-down values of typical experimental parameters. Thus Figs. 2–4, discussed below, were obtained with the following parameters: $l = 0.5$ mm, $d = 0.14$ mm, $\theta_2 = 4.0$ deg, $\theta_4 = 5.0$ deg, $\theta_D = 12$ deg, $I_{er} = 0.01$, radiation wavelength $\lambda = 0.514$ μ m, and refractive index $n = 2.4$. Typical runs were conducted on a 3000 (along y) \times 300 (along x) grid, with the width of the calculation region along the y coordinate being given by $l_y = (2.5 - 4)d$. The penalty for using a scaled-down length l is that the effects of diffraction are exaggerated. In particular, the diffraction of a pumping beam having several separated strong Fourier harmonics into higher orders is larger than it would be for larger values of l .

3. NUMERICAL RESULTS

Figures 2(a)–2(c) depict the transmissivities T and the conjugation fidelities H in the geometry of the DPCM as functions of the nonlinearity $\gamma_0 l$ for different values of

random seeds ϵ equal to 10^{-4} , 10^{-6} , and 0, respectively (the last case denotes no random seeding). Figure 2(d) shows the time evolution of the transmissivities and the conjugation fidelities for $\epsilon = 10^{-4}$ and $\gamma_0 l = 8$. The parameter ϵ is defined as the ratio of the average intensity of noise in Fourier space to the maximum intensity of the Fourier spectrum of the copropagating pump. The forward-propagating pump beam A_4 is a cosine-modulated Gaussian beam propagating at an angle $\theta_4 = 5$ deg with the form factor $B_{4,in}(y) \propto \cos[20\sqrt{2}(y - y_4)/d]$, corresponding to an angular divergence $\delta\theta \approx 0.8$ deg. The backward-propagating pumping beam A_2 is a speckle beam propagating at an angle $\theta_2 = 4$ deg with a divergence $\delta\theta \approx 2.3$ deg. Both beams have the same powers. Figure 2(d) shows the temporal dynamics of the reflectivities and the conjugation fidelities for $\epsilon = 10^{-4}$.

Figure 2 shows that the reflectivity and the conjugation fidelity in the geometry of the DPCM are directly dependent on the level of seeding. The reflectivity and the conjugation fidelity both increase as the level of seeding is increased. In general, they also grow with an increase in nonlinearity, as expected. We also performed calcula-

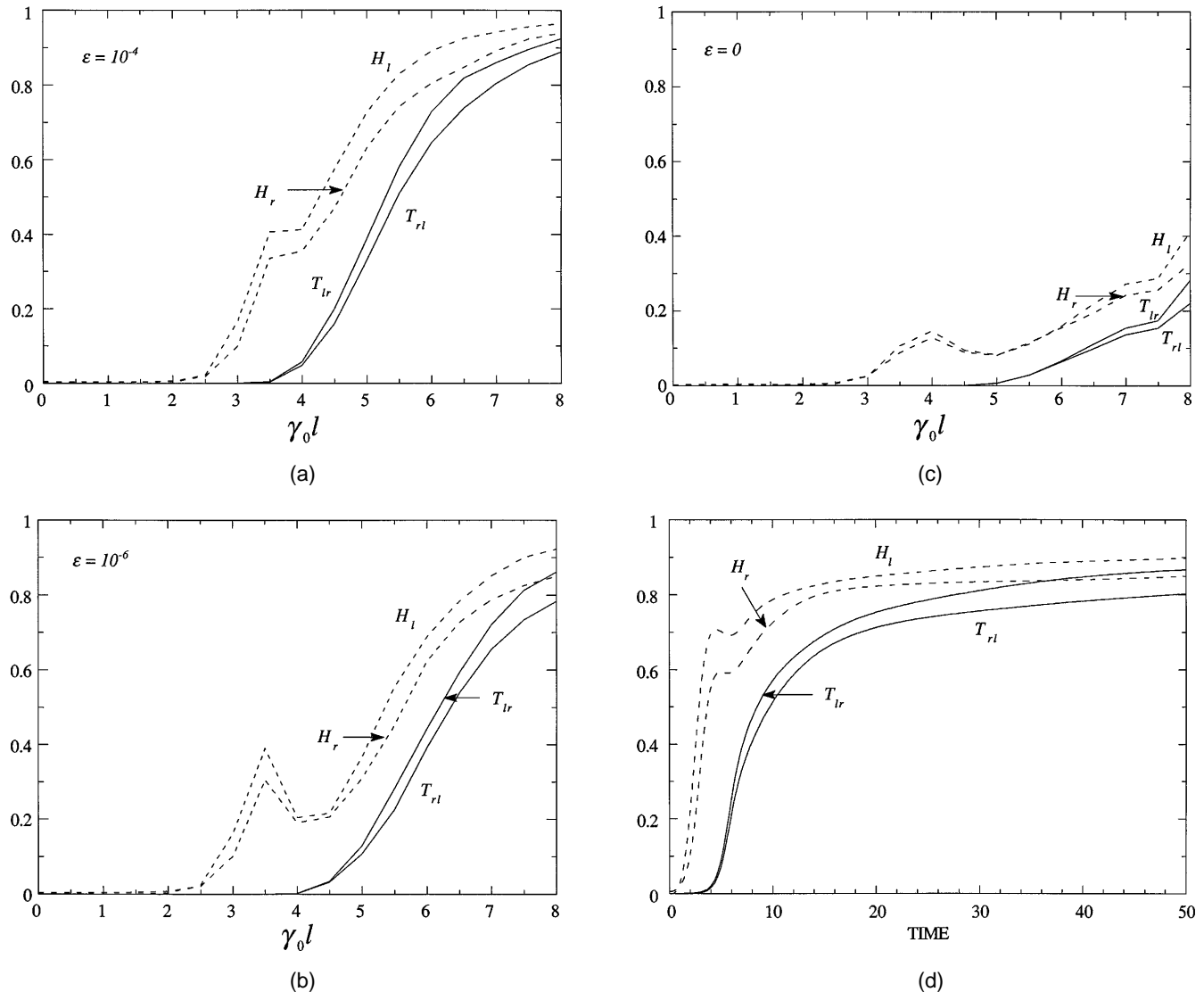


Fig. 2. Transmissivities (T_{rl} , T_{lr}) and conjugation fidelities (H_r , H_l) as functions of nonlinearity for levels of random seeding noise (a) $\epsilon = 10^{-4}$, (b) 10^{-6} , and (c) 0. (d) Time evolution of the transmissivities and the conjugation fidelities for $\epsilon = 10^{-4}$ and $\gamma_0 l = 8$.

tions for cases in which both beams had regular structure or were speckle beams. The results were similar to those presented in Fig. 2.

The peculiarities in the behavior of the conjugation fidelities at low values of reflectivities in Figs. 2(b) and 2(c) are a physical effect resulting from restructuring of the spatial distributions of the scattered beams. The restructuring is due to different gratings written by the pumping beams and the noise, competing for the energy of the pumps, when the scattered beams grow. However, the particular values of H_r and H_l in this region should not be taken too literally because both absolute and relative values of the conjugation fidelities for small levels of transmissivity are dependent on the particular realization of the seeding noise, the spatial distributions of the pumping beams, and the width of the window in Fourier space chosen to select the pumping and the scattered beams. One should also keep in mind that the nonlinear transmissivities shown in these figures were obtained by integration of all radiation within a certain solid angle around the nominal directions of propagation of the scattered beams and thus include contributions from both conjugate and nonconjugate parts. Low values of fidelity mean that most of this radiation is amplified noise. A good estimate of the conjugate part is given by the product of the transmissivity and the corresponding fidelity.

Figures 3 and 4 depict distributions of the pumping and the scattered beams in both Fourier and coordinate space for $\gamma_0 l = 7$ and $\epsilon = 10^{-6}$, with all the other parameters as in Fig. 2. Figure 3(a) shows the spectral intensity of the input signal beam A_3 (noise, dotted-dashed curve), the output spectral intensity of the same signal beam (solid curve), and the input spectral intensity of the counterpropagating Gaussian-cosine pump beam A_4 (dashed curve). The divergence of the input pump beam A_4 (the separation between the two maxima in the spectrum) is equal to ≈ 0.8 deg. Figure 3(b) shows spectral distributions of the output signal beam A_1 and the counterpropagating input speckle pump beam A_2 . In Fig. 3 the spectra of the input pumps are inverted to facilitate direct comparison with the spectra of the scattered beams. The width of the Fourier window in both Figs. 3(a) and 3(b) is equal to the input divergence of the speckle pump, ≈ 2.3 deg.

These figures demonstrate that the small-scale structure of the pumps is accurately reproduced. The physical reason for this is diffraction, which allows the nonlinear interaction selectively to amplify those spectral components of the input noise distribution that correspond to the spectral components of the counterpropagating pumping beams. Without diffraction nonconjugate spectral components of the input noise distribution would also be amplified, resulting in lower conjugation fidelity. Notice that there are large-scale distortions in the Fourier spectra of the output scattered beams. The physical meaning of these distortions can be seen best in coordinate space.

Figure 4(a) shows the output distribution of the scattered beam A_3 (solid curve) and the input distribution of the counterpropagating pump beam A_4 (dashed curve) in coordinate space. It demonstrates reproduction of the fine structure of pump $A_{4,in}$ by the scattered beam, accompanied by large-scale distortions of the envelope. These distortions are a clear signature of the effects of the non-

collinearity of the interacting beams and are in full agreement with predictions stated in previous papers.^{5,6} The distortions are due to the convective flow of energy out of the interaction region in the direction of the common component of the group velocities of the scattered beams (from bottom to top of Fig. 1). Figure 4(b) shows the output intensity distribution of the scattered beam A_1 together with the input distribution of the counterpropagating pump A_2 and again clearly demonstrates large-scale distortions that are due to convection. Figure 4(c) shows input (dashed curve) and output (solid curve) intensity distributions of the Gaussian-cosine pump beam A_4 . Figure 4(d) shows input and output distributions of the speckle pump beam A_2 . When the pumping beams propagate at angles θ_l with respect to the x axis they experience a transverse displacement $\theta_l l$. We removed this transverse displacement from Figs. 4(c) and 4(d) by shifting the output intensity distributions by the amount $-\theta_l l$. Note that no adjustments were necessary in Figs. 4(a) and 4(b) because each of these figures depicts pairs of beams on the same side of the nonlinear medium. Figures 4(c) and 4(d) show that the output profiles of the pumping

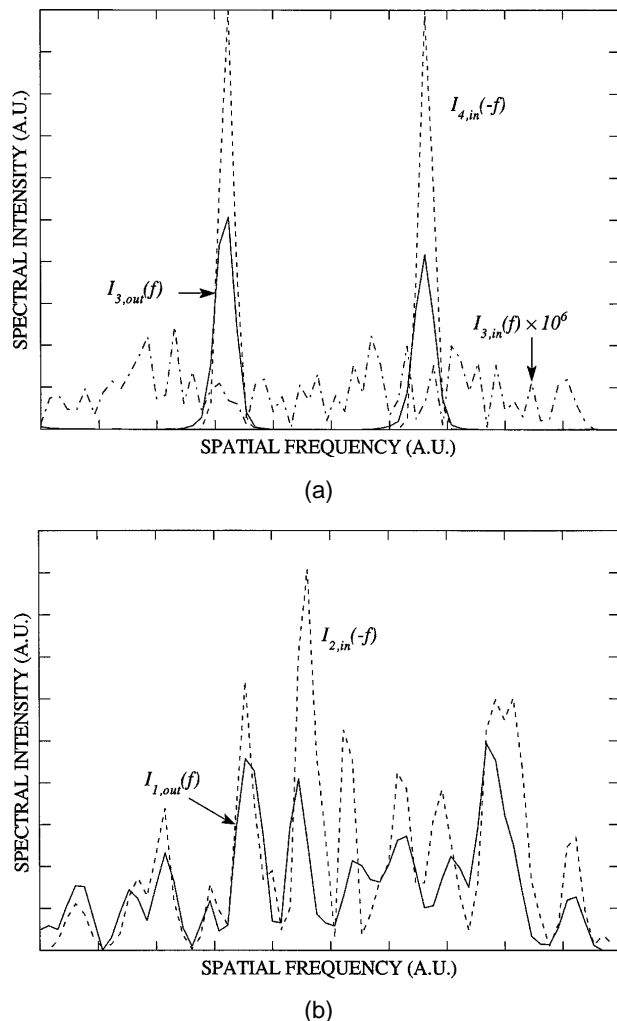


Fig. 3. Fourier power spectra of the interacting fields: (a) input and output scattered beam A_3 and counterpropagating input pump beam A_4 , (b) output scattered beam A_1 and input counterpropagating pump beam A_2 . The width of the depicted region corresponds to an angular window covering 2.3 deg.

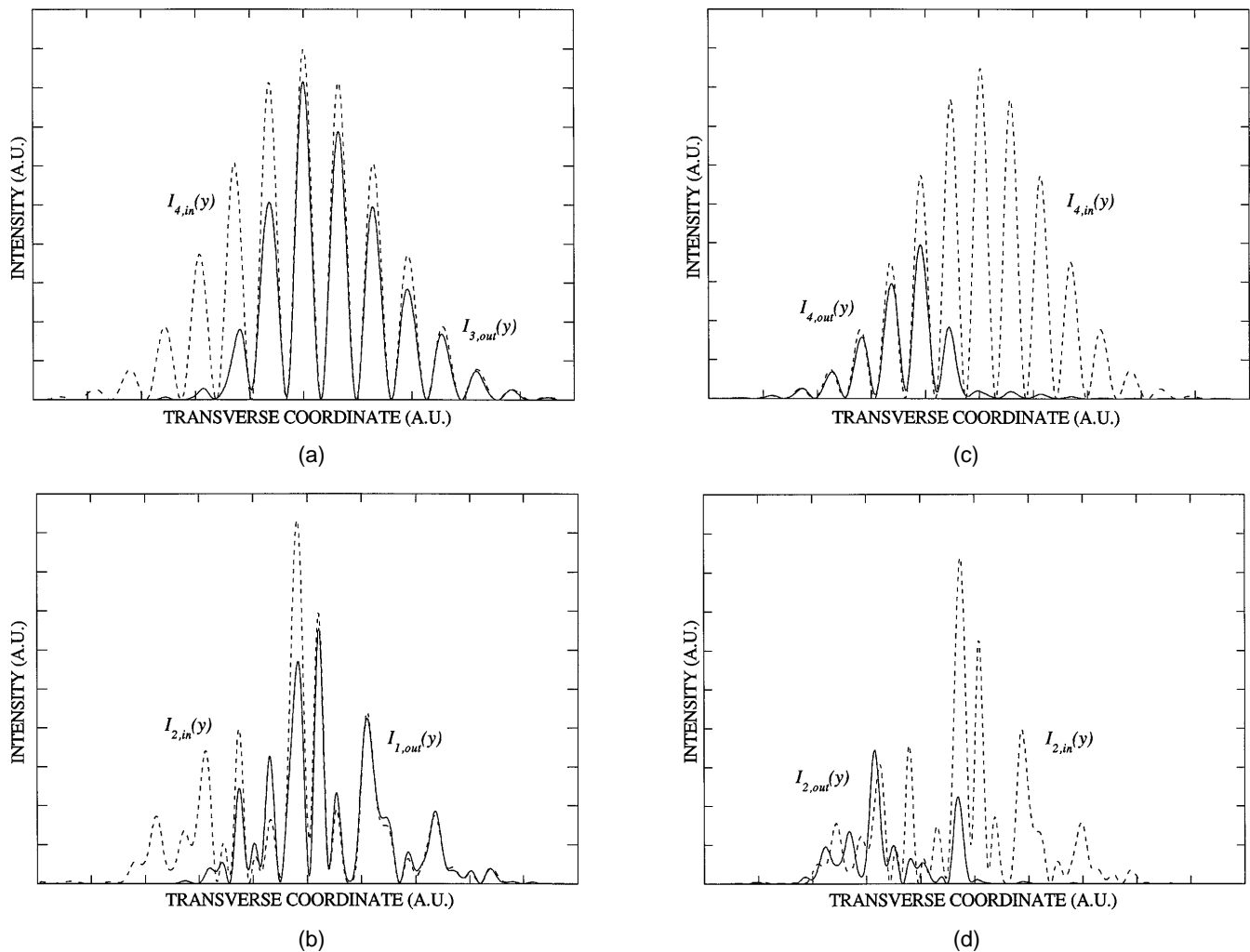


Fig. 4. Intensity distributions of the interacting fields: (a) output scattered beam A_3 and counterpropagating input pump beam A_4 , (b) output scattered beam A_1 and input counterpropagating pump beam A_2 , (c) input and output pump beam A_4 , (d) input and output pump beam A_2 .

beams emerging from the nonlinear medium after interaction are predominantly depleted on the side where the intensities of the output scattered beams [see Figs. 4(a) and 4(b)] are larger. The width of the region depicted in Figs. 4(a)–4(d) is equal to $\sim 70\%$ of the total computational window along the y coordinate.

To prove the point that the direction of convective flow of the scattered beams is determined by that of the common component of their group velocities and not by the boundaries of the medium, we conducted several runs with pumping beams whose wave-vector y components had different signs. In these runs one of the pumps had a negative y component of its group velocity (positive value of the incidence angle θ_l), and the other one had a positive component (negative value of θ_l). All the runs demonstrated characteristic spatial shifts of the intensity distributions of the scattered beams with respect to those of the counterpropagating pumps because of convection effects. The direction of this shift was always determined by the sign of $\theta_2 + \theta_4$, i.e., by the sign of the sum of the group velocities of the scattered beams.

Figure 2 shows strong dependence of both the transmissivities and the conjugation fidelities in the geometry of the DPCM on the level of seeds. It is instructive to

consider Fig. 2(c) ($\epsilon = 0$) in more detail because in this case the seeds (not random) are supplied by the pumping beams themselves. First, the Fourier spectrum of any pumping beam in general contains all spatial frequencies, including those corresponding to the direction of propagation of the copropagating scattered beam. The second, and more important, point is that a beam propagating through a nonlinear medium generates new spatial frequencies because of self-interaction. The level of the generated spatial frequencies increases as the nonlinearity increases. This second source of seeds cannot be eliminated because, even if spatial frequencies corresponding to the direction of propagation of the scattered beams are artificially cleared out at the input, they appear at the output.

To illustrate the above points we propagate a single Gaussian-cosine pump beam A_4 with everything else switched off (no random seeds, no pump beam A_2) through the photorefractive medium at the level of nonlinearity $\gamma_0 l = 8$ and with all the other parameters being the same as for Figs. 2–4. The input and the output Fourier spectra of the beam on a logarithmic scale are given in Fig. 5. Figure 5(a), representing the input spectrum of pump beam A_4 , shows that even without external seeding

the input level of seeds in the direction of the scattered beam is approximately 10^{-9} . This level is much higher than the one that would follow from analytical Fourier transformation of this pump field and is determined mainly by the width of the calculation region l_y . Thus changing this width from $l_y = 2.5d$ to $l_y = 3.6d$, for example, lowers the level of seeds in the direction of the scattered beam A_1 to $\approx 10^{-14}$. The reason is that the discrete Fourier transform implies that a function being transformed is periodic in y with the period l_y , so the wings of the pumping beam in coordinate space are truncated. The analytical Fourier spectrum is recovered in the limit of infinitely large l_y . Figure 5(b) represents the output spectrum of the same beam, showing the appearance of a broad low-intensity pedestal that is due to distorted replication of the two-humped Fourier spectrum of the input beam shown in Fig. 5(a). The level of seeds in the direction of the scattered beam A_1 has grown from $\approx 10^{-9}$ to almost $\approx 10^{-2}$. Cutting off the low-intensity wings in the input spectral distribution of the pump beam A_4 did not result in noticeable changes in the output spectrum. The effective level of seeds in the presence of the second pumping beam is much smaller, but Fig. 5

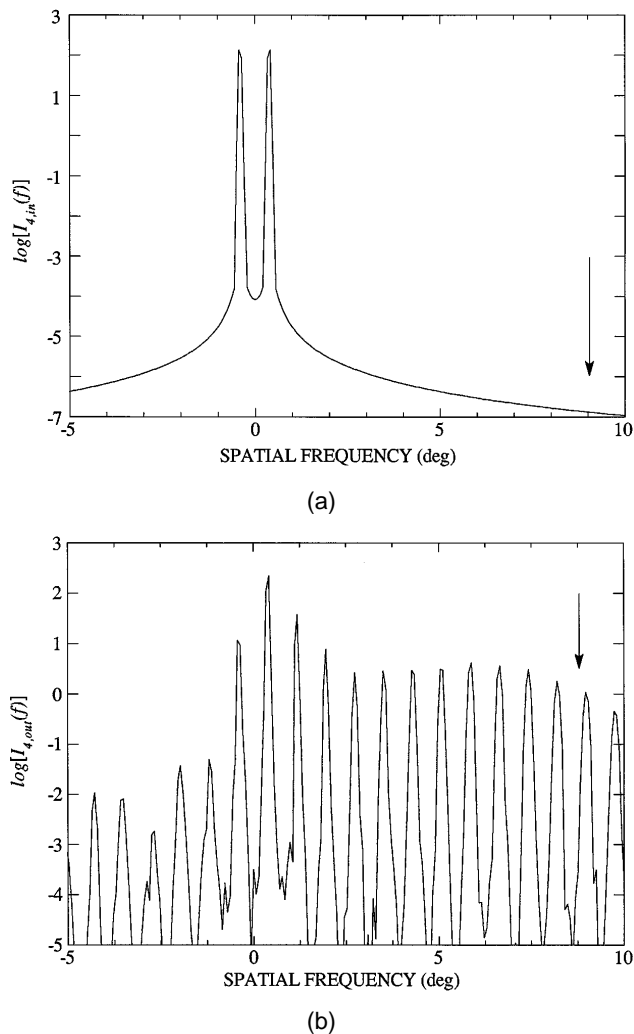


Fig. 5. Fourier power spectra of (a) input and (b) output single pump beam A_4 in the absence of the second pump and no random seeding for $\gamma_0 l = 8.0$. The downward-pointing arrows indicate the direction of propagation of the corresponding scattered beam.

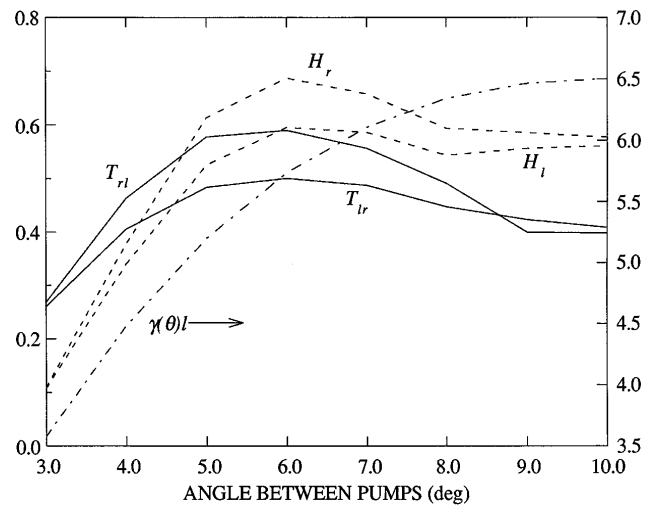


Fig. 6. Transmissivities (T_{rl} , T_{lr}) and conjugation fidelities (H_r , H_l) as a function of the angle between the pumping beams. The dashed-dotted curve is the local coupling coefficient $\gamma(\theta)l$.

illustrates the fact that the appearance of these seeds is unavoidable. There are two reasons for the appearance of the repetitive spectral structure in Fig. 5(b). First, the nonlinear material equation (3) generates higher spatial harmonics of the grating formed by the two maxima in the input Fourier spectrum of pump beam A_4 . Second, the Bragg-mismatch parameter for multiple scattering off this grating is equal to $\Delta kl = kl(\delta\theta)^2 \approx 2.7$, so the grating is thin. Note that the transition to larger values of l will increase the Bragg-mismatch parameter and will suppress generation of higher orders of diffraction. Because all beams have finite spectral widths, it matters little whether a maximum or a minimum of the spectrum shown in Fig. 5(b) coincides exactly with the direction of propagation of the scattered beam. Because the Bragg-mismatch parameter corresponding to a transition from one maximum of the Fourier spectrum to an adjacent one is small, the system draws seeds from the closest maximum.

Note that the above two reasons for the generation of seeds pertain to the physics of the DPCM. One cannot exclude the further possibility that some part of the scattering shown in Fig. 2(c) for high values of $\gamma_0 l$ is due to numerical noise. For high-amplification coefficients pd [Eq. (1)] in the transverse direction it is increasingly difficult to guarantee that all possible sources of parasitic seeding resulting from the finite width of the calculation window are eliminated.

Figure 6 shows transmissivities (solid curves) and conjugation fidelities (dashed curves) in the geometry of the DPCM as functions of the angle between the pump beams; the dashed-dotted curve is the coupling coefficient $\gamma(\theta)l$ defined by Eq. (4). Both pumps are equal-power speckled beams with $d = 0.14$ mm and randomly generated input spectra of compact support corresponding to equal angular divergencies $\delta\theta \approx 2.3$ deg, nonlinearity parameter $\gamma_0 l = 6.5$, $\theta_g = 10$ deg, and $\epsilon = 10^{-6}$. The angle of incidence of pump beam A_4 was held equal to $\theta_4 = 4$ deg, whereas that of pump beam A_2 was changed from $\theta_2 = -1$ deg for $\theta_2 = 6$ deg. Figure 6 shows that nonlinear scattering for small angles between the pump-

ing beams is characterized by low values of conjugation fidelity combined with relatively large values of transmissivity. This result indicates that the effective seeds in this region considerably exceed ϵ and are supplied predominantly by the nonlinearly widened spectra of the pumps. These seeds are too large and cannot be transferred into conjugate radiation by the relatively moderate nonlinearity [$\gamma(\theta)l \approx 3.5$ for $\theta = 3$ deg]. Increasing the value of θ increases both the transmissivities and the fidelities, which pass through a shallow maximum and then remain at relatively high levels. Note, in contrast, that the nonlinear coupling coefficient $\gamma(\theta)l$ grows monotonically with increasing θ in Fig. 6. Turning the random seeds off ($\epsilon = 0$) has a more pronounced effect, the larger the angle between the pumps. Thus, for example, both transmissivities and conjugation fidelities show almost no change for $\theta = 3$ deg and drop down approximately 2–2.5 times for $\theta = 10$ deg. There are two reasons for the shallow maximum shown in Fig. 6. First, as we have discussed in Section 1 in connection with Eq. (1), the two-dimensional model of the DPCM⁴⁻⁶ predicts that maximum values of transmissivities take place for $\theta < \theta_D$. Figure 6 provides numerical confirmation of this prediction in the presence of diffraction. Second, the total level of seeds in the directions of the scattered beams (random plus those from pump spectra) is larger for smaller angles between the pumping beams. In principle, there is a third reason for the shallow maximum: the effective overlap region of the beams gets smaller for larger values of θ , but for the parameters of Fig. 6 this effect is not important.

As has been discussed above, the two-dimensional physics of the DPCM is due to the finite size of the interaction region in the transverse dimension. The failure to account properly for this circumstance leads to wrong results. To illustrate this point we conducted parallel calculations with two sorts of pump. The first choice corresponded to the modulated Gaussian beams:

$$A_{4,\text{in}}(y) = [1 + \cos(10\pi y/d)] \exp[-i\theta_4 k y - 4(y - y_4)^2/d^2], \quad (7a)$$

$$A_{2,\text{in}}(y) = [1 - \cos(14\pi y/d)] \exp[-i\theta_2 k y - 4(y - y_2)^2/d^2]. \quad (7b)$$

The second choice corresponded to the same modulation but without the Gaussian envelopes:

$$A_{4,\text{in}}(y) = [1 + \cos(10\pi y/d)] \exp(-i\theta_4 k y), \quad (8a)$$

$$A_{2,\text{in}}(y) = [1 - \cos(14\pi y/d)] \exp(-i\theta_2 k y). \quad (8b)$$

The steady-state transmissivities T and the conjugation fidelities H as functions of the nonlinearity $\gamma_0 l$ for the modulated Gaussian pumps [Eqs. (7)] are presented in Fig. 7. The parameters for this figure are $l = 1.5$ mm, $d = 0.3$ mm, $\theta_4 = 4.5$ deg, $\theta_2 = 3.5$ deg, $\theta_D = 10$ deg, $\lambda = 0.514$ μm , $I_{\text{er}} = 0.01$, and $n = 2.3$. The calculations were conducted by the FFT method on a 4000 (along y) \times 200 (along x) grid, with the width of the calculation region along the y coordinate being given by $l_y = 3d$. The two sets of curves correspond to the values of the random seeds ϵ equal to 10^{-5} and 10^{-12} . The transmissivities

T_{1r} , T_{r1} and the conjugation fidelities H_r , H_l are near each other, so only one pair is shown.

The values of the transmissivities and the conjugation fidelities for the pumping beams [Eqs. (7)] look similar to those shown in Fig. 2. They exhibit a strong dependence on the level of seeds, consistent with the convective nature of the instability in the geometry of the DPCM. The transverse distributions of the scattered beams demonstrate the same reproduction of the small-scale structure and the large distortions of the envelopes that are due to convection effects, as in Fig. 4. The value of the relative transverse displacement of the beams $(\theta_2 + \theta_4)l/d$ is larger for the parameters of Fig. 7 than for those of Fig. 2. In other words, a larger part of the rhombus-shaped beam-overlap region lies inside the nonlinear medium. This is why the nonlinearity necessary for reaching a certain value of the transmissivities is higher in Fig. 7 than in Fig. 2.

Calculations with the transversely unbounded pumps [Eqs. (8)] with the same parameters as in Fig. 7 resulted in the onset of scattering near $\gamma_0 l \approx 3$ for both values of seeding and in the loss of stability of the stationary solutions near $\gamma_0 l \approx 4$. The value of the nonlinearity corresponding to the loss of stability was found to depend on the ratio l_y/l of the width of the calculation window to the length of the medium. A twofold reduction in l_y increased the region of existence of stationary solutions up to $\gamma_0 l \approx 5.5$; a fourfold reduction, to $\gamma_0 l \approx 8.5$. Figure 8 shows the transmissivities T and the conjugation fidelities H as functions of the nonlinearity $\gamma_0 l$ for the transversely unbounded pumps [Eqs. (8)] carried out for $l_y = 3d/4$ (four times less than in Fig. 7). The number of transverse points was also decreased four times to preserve the same spatial resolution.

The behavior of the transmissivities and the conjugation fidelities for pumps [Eqs. (8)] is completely different from that shown in Fig. 7. Thus the output characteristics are weakly dependent on the level of seeds, there exists a well-defined threshold of scattering ($\gamma_0 l \approx 3$ for the chosen pumps), and the output transmissivities remain nonzero above this threshold even when the seeds

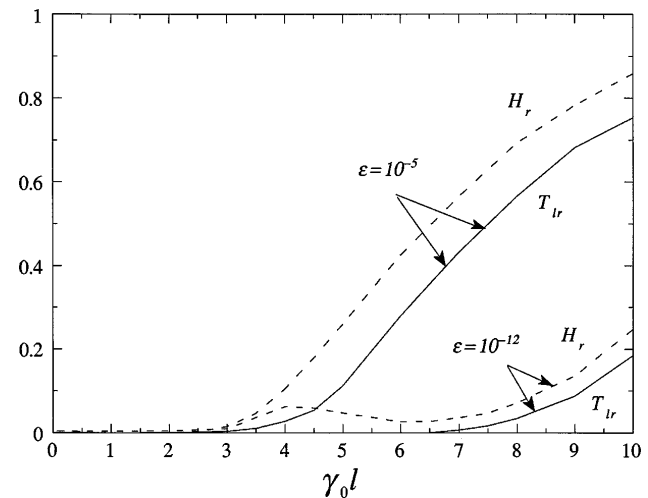


Fig. 7. Transmissivities T_{1r} and conjugation fidelities H_r as functions of the nonlinearity for the transversely bounded pumping beams described by Eqs. (7) and for levels of random seeding $\epsilon = 10^{-5}$, 10^{-12} . The length of the nonlinear medium equals 1.5 mm.

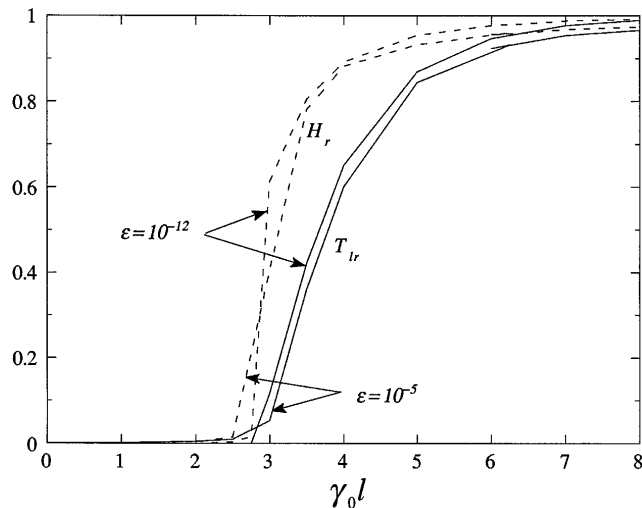


Fig. 8. Same as in Fig. 7 but for the transversely unbounded pump beams described by Eqs. (8).

are essentially switched off. All these features are indicative of an absolute (oscillation) instability. Note also that the transmissivities and the conjugation fidelities shown in Fig. 8 for $\epsilon = 10^{-5}$ start to grow slightly earlier than do those for $\epsilon = 10^{-12}$, but for large coupling constants the situation changes. Both the transmissivities and the conjugation fidelities for $\epsilon = 10^{-12}$ lie higher than those for $\epsilon = 10^{-5}$. This degradation in the performance of the DPCM for a higher level of seeds (increased fanning) was predicted in Ref. 18 (see Fig. 3 therein) during consideration of the influence of fanning on the characteristics of the DPCM in the framework of a one-dimensional model. Figure 8 thus demonstrates that the physics of the DPCM for the pumps [Eqs. (8)] is well described by the one-dimensional model.

The reason for the differences between the characteristics of the DPCM for pumps [Eqs. (7) and (8)] is that the pumps [Eqs. (7)] are real beams, whereas Eqs. (8) describe structures that are unbounded in the transverse dimension. All the two-dimensional effects discussed above that are due to the finite size of the interaction region in the transverse dimension are lost for such structures.

All numerical calculations are carried out with a finite number of transverse points and a calculation window of finite size in the transverse dimension. To describe properly the two-dimensional physics of the DPCM in numerical calculations care should be taken that the electromagnetic fields are confined within the calculation window throughout the interaction region (for any value of the longitudinal coordinate) and do not touch the boundaries both in coordinate and in Fourier space. When this condition is violated, as is the case for pumps [Eqs. (8)], the boundary conditions impart a strong parasitic influence and completely change the physics compared with that describing the behavior of real beams.

4. CONCLUSIONS

We analyzed numerically the geometry of the double phase-conjugate mirror in the framework of a two-dimensional model. The model is based on parabolic

equations for the electromagnetic radiation and on nonlinear material equations that are exact within the paraxial approximation. It takes into account diffraction and noncollinearity of the interacting beams and their finite size. We investigated the geometry of the DPCM in the cases of pumping beams with regular structure and of speckled beams. We confirmed the predictions of Refs. 5 and 6 that the DPCM is an amplifier, with the output level of the scattered beams being directly dependent on the level of their input seeds. We investigated the dependence of the nonlinear transmissivities and the conjugation fidelities on the level of these seeds. In the absence of random seeding the seeds are supplied by the spectra of the pumps, which are nonlinearly broadened because of self-interaction for large values of the nonlinearity. The physical reason that turns the geometry of the DPCM into an amplifier is the noncollinearity of the interacting beams and the finite size of the interaction region in all directions. Convective transport of energy in the direction of the common component of the group velocity of the noncollinear scattered beams creates a channel of losses out of the finite-sized interaction region. The only mechanism that can potentially counterbalance these losses is diffraction. When the angle between the pumps and the copropagating scattered beams is larger than the characteristic diffraction divergence angle of the interacting beams the convective mechanism dominates, quenching the oscillation instability. A clear signature of convective effects is large-scale distortions of the amplitudes of the interacting beams. These distortions correspond to the displacement of the transverse intensity distributions of the output scattered beams in the direction of the common component of their group velocity. These distortions are more pronounced for relatively moderate values of the nonlinearity and become less noticeable when the pumping beams are completely depleted for large nonlinearities. The small-scale structure of the pumping beams is reproduced.

In conclusion, we direct the reader's attention to several recent papers⁸⁻¹² that claim to analyze the geometry of the DPCM in the framework of two-dimensional models. In our opinion these papers missed the essence of the two-dimensional nature of the DPCM.

Inspection of Refs. 8-10 immediately reveals that the pumping beams in these papers are taken as plane waves. The ensuing equations for scattered beams are linear, are decomposable into a set of completely decoupled equations for Fourier harmonics, and contain none of the two-dimensional effects that are due to the finite size of the interaction region, discussed in Refs. 4-6. An additional claim made in Refs. 8-10 is that abandoning the slowly varying envelope approximation (SVEA) qualitatively changes the behavior of the DPCM compared with that from SVEA-based approaches. To examine this claim in more detail consider Eqs. (16) of Ref. 10:

$$\left(\frac{d^2}{dx^2} + 2ik_x \frac{d}{dx} \right) A_1 = 2ik_x \frac{\gamma}{I} (A_1 A_4^* + A_2^* A_3) A_4, \quad (9a)$$

$$\left(\frac{d^2}{dx^2} - 2ik_x \frac{d}{dx} \right) A_3 = 2ik_x \frac{\gamma}{I} (A_1 A_4^* + A_2^* A_3) A_2. \quad (9b)$$

These equations describe evolution of the scattered plane waves A_1 and A_3 in the field of undepleted pumps A_2 and A_4 in the TE case; A_1 exactly counterpropagates A_2 , and A_3 counterpropagates A_4 . We obtain the SVEA equations from Eqs. (9) by dropping the second derivatives. According to Refs. 8–10, Eqs. (9) do not have solutions corresponding to an absolute instability, i.e., solutions that have poles in the complex-frequency plane corresponding to an exponential growth of perturbations. This conclusion is incorrect. Indeed, if we restrict ourselves to the consideration of a transmission grating, we must consider $A_1(x=0)$, $A_3(x=l)$, $\partial A_1(0)/\partial x$, and $\partial A_3(l)/\partial x$ as independent boundary conditions. Solution of Eqs. (9) then results in the dispersion equation

$$\kappa_1(\kappa_3 - \kappa_2)B_2B_3 + \kappa_2(\kappa_1 - \kappa_3)B_1B_3 + \kappa_3(\kappa_2 - \kappa_1)B_1B_2 = 0, \quad (10a)$$

$$B_l = \frac{(1+q)\sqrt{q}}{2ik_x\gamma} \left(\kappa_l^2 + 2ik_x\kappa_l - \frac{2ik_x\gamma}{1+q} \right) \exp(\kappa_l l) + \sqrt{q}, \quad (10b)$$

where κ_l are the roots of the equation $\kappa^3 + (4k_x^2 - 2ik_x\gamma)\kappa - 4k_x^2\gamma(1-q)/(1+q) = 0$. Dispersion equation (10) reduces to the familiar equation $q \exp[\gamma l(1-q)/(1+q)] = 1$, determining the threshold of the DPCM in the one-dimensional SVEA case. The corrections to this equation that are due to the inclusion of non-SVEA terms are of the order of $\gamma l/k_x l \ll 1$.

Inspection of Refs. 11 and 12 reveals that the pump beams in these papers were chosen to be unbounded infinite-extent periodic structures of the form

$$A_{2(4),in} \sim \exp[ik\theta_{2(4)}y][1 + a_{2(4)} \cos(2\pi y/l_g) + b_{2(4)} \cos(4\pi y/l_g)], \quad (11)$$

where $\theta_{2,4}$ are the angles of incidence, a and b are coefficients of the order of unity, and l_g is some scaling length. The conclusions of Refs. 11 and 12 are that the DPCM is an oscillator “since there is a well-defined threshold equal to 2,” and above this threshold “one can turn off the noise ... and the DPCM remains essentially unchanged.” These conclusions are correct for the pumps described by relation (11). Equally correct is the fact that relation (11) has nothing to do with real, bounded beams. The relevant physics was discussed above in connection with Fig. 8.

ACKNOWLEDGMENT

This research was supported by National Science Foundation grant PHY90-12244 and by the Optoelectronic Com-

puting Systems Center, a National Science Foundation Engineering Research Center.

*Present address, Department of Optics and Fluid Dynamics, Risø National Laboratory, DK-4000 Roskilde, Denmark.

REFERENCES

1. S. Weiss, S. Sternklar, and B. Fischer, “Double phase-conjugate mirror: analysis, demonstration, and applications,” *Opt. Lett.* **12**, 114–116 (1987).
2. B. Fischer, S. Sternklar, and S. Weiss, “Photorefractive oscillators,” *IEEE J. Quantum Electron.* **25**, 550–569 (1989).
3. N. M. Kroll, “Excitation of hypersonic vibrations by means of photoelastic coupling of high-intensity light waves to elastic waves,” *J. Appl. Phys.* **36**, 34–40 (1965).
4. A. A. Zozulya, V. P. Silin, and V. T. Tikhonchuk, “The theory of phase conjugation during stimulated scattering in a self-intersecting light beam,” *Sov. Phys. JETP* **65**, 443–449 (1987).
5. A. A. Zozulya, “Double phase-conjugate mirror is not an oscillator,” *Opt. Lett.* **16**, 545–547 (1991).
6. V. T. Tikhonchuk and A. A. Zozulya, “Structure of light beams in self-pumped four-wave mixing geometries for phase conjugation and mutual conjugation,” *Prog. Quantum Electron.* **15**, 231–293 (1991).
7. A. A. Zozulya, M. Saffman, and D. Z. Anderson, “Propagation of light beams in photorefractive media: fanning, self-bending, and formation of self-pumped four-wave mixing geometries,” *Phys. Rev. Lett.* **73**, 818–821 (1994).
8. K. D. Shaw, “The double phase conjugate mirror is an oscillator,” *Opt. Commun.* **90**, 133–138 (1992).
9. K. D. Shaw, “Vector versus scalar theory of the double phase conjugate mirror,” *Opt. Commun.* **94**, 458–468 (1992).
10. K. D. Shaw, “Operation of the double phase conjugate mirror for TE polarization: exact solution and failure of the slowly varying envelope approximation,” *Opt. Commun.* **103**, 326–338 (1993).
11. M. Segev, D. Engin, A. Yariv, and G. Valley, “Temporal evolution of photorefractive double phase conjugate mirror,” *Opt. Lett.* **18**, 1828–1830 (1993).
12. D. Engin, M. Segev, S. Orlov, A. Yariv, and G. Valley, “Double phase conjugation,” *J. Opt. Soc. Am. B* **11**, 1708–1717 (1994).
13. N. V. Kukhtarev, V. B. Markov, S. G. Odoulov, M. S. Soskin, and V. L. Vinetskii, “Holographic storage in electrooptic crystals: I. Steady state,” *Ferroelectrics* **22**, 949–960 (1979).
14. T. J. Hall, R. Jaura, L. M. Connors, and P. D. Foote, “The photorefractive effect: a review,” *Prog. Quantum Electron.* **10**, 77–146 (1985).
15. M. Cronin-Golomb, “Whole beam method for photorefractive nonlinear optics,” *Opt. Commun.* **89**, 276–282 (1992).
16. L. Sun and G. L. Yip, “Modified finite-difference beam-propagation method based on the Douglas scheme,” *Opt. Lett.* **18**, 1229–1231 (1993).
17. D. Yevick and B. Hermansson, “New formulations of the matrix beam propagation method: application to rib waveguides,” *IEEE J. Quantum Electron.* **25**, 221–229 (1989).
18. A. A. Zozulya, “Fanning and photorefractive self-pumped four-wave mixing geometries,” *IEEE J. Quantum Electron.* **29**, 538–555 (1993).